



Study on the Structure of Cu/ZrO₂ Catalyst and the Formation Mechanism of Disodium Iminodiacetate and Sodium Glycine

Yongsheng Wang^{1,2} · Hongwen Zhu¹ · Zhengkang Duan^{1,2} · Zhenzhen Zhao^{1,2} · Yunlu Zhao^{1,2} · Xiaolin Lan¹ · Li Chen¹ · Dongjie Guo¹

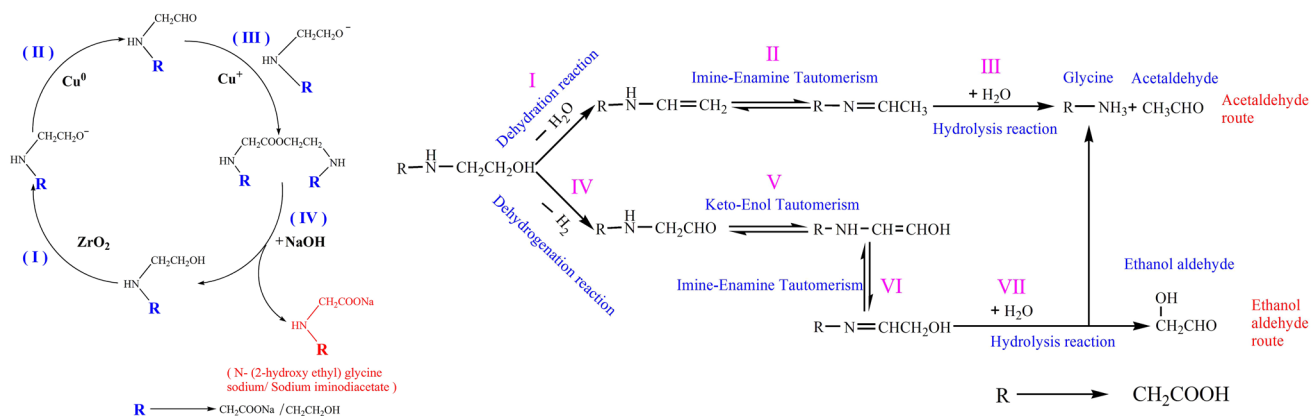
Received: 2 July 2019 / Accepted: 3 October 2019
© Springer Science+Business Media, LLC, part of Springer Nature 2019

Abstract

A new method to prepare Cu/ZrO₂ catalysts by reducing CuO/ZrO₂ with hydrazine hydrate is reported, and the prepared catalysts were used to synthesize disodium iminodiacetate by diethanolamine dehydrogenation. Hydrazine hydrate can rapidly reduce the CuO/ZrO₂ precursor powder in an alkaline environment at a moderate temperature. The ratio of Cu⁰/Cu⁺ at the Cu/ZrO₂ surface was controlled by the amount of hydrazine hydrate and the reduction reaction time. The formation mechanism of disodium glycine as the main byproduct and iminodiacetate were deduced by investigating the product yield, the reaction time, and the presence of acetaldehyde in the evolved gas. It has been shown that the ratio of Cu⁰/Cu⁺ in Cu/ZrO₂ significantly affects the dehydrogenation of diethanolamine into disodium iminodiacetate. Cu⁰ and Cu⁺ are the catalytic activity centers in the dehydrogenation of diethanolamine which respectively produce intermediate aldehydes and an ester via nucleophilic addition reactions. The formation mechanism of sodium glycinate is related to the tautomerism of intermediate products and Schiff base hydrolysis.

Graphic Abstract

The formation mechanism of disodium iminodiacetate and sodium glycine producing by the dehydrogenation of diethanolamine over the Cu/ZrO₂ catalysts which were prepared by a new reduction method.



Keywords Copper-zirconium catalysts · Diethanolamine · Disodium iminodiacetate · Reaction mechanism · Hydrazine hydrate

Electronic supplementary material The online version of this article (<https://doi.org/10.1007/s10562-019-02989-z>) contains supplementary material, which is available to authorized users.

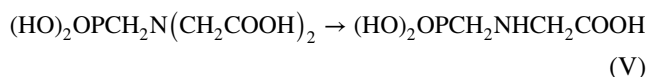
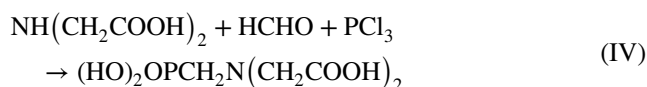
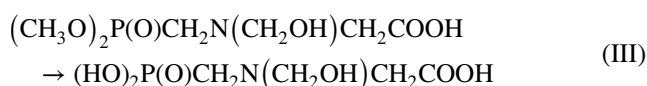
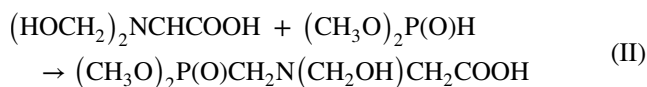
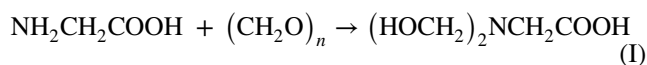
✉ Zhengkang Duan
dzk0607@163.com

Extended author information available on the last page of the article

1 Introduction

Glyphosate is widely used as a broad spectrum, efficient, and environmentally friendly pesticide [1] that is typically obtained by one of two main industrial routes: (I–III) the

glycine (Gly) route and (IV–V) the iminodiacetic acid (IDA) route [2]. The iminodiacetic acid route usually involves transforming IDA, formaldehyde, phosphoric acid, and other reactants into *N*-(phosphonomethyl) iminodiacetic acid hydrate (PMIDA), which is then oxidized to obtain glyphosate. Currently, using diethanolamine (DEA) dehydrogenation to synthesize IDA is the most environmentally-friendly and safe process [3].



DEA reacts with NaOH in an autoclave at 160–180 °C and a pressure of 1–2 MPa over Cu-based catalysts to produce disodium iminodiacetate, which is then purified by acidification to obtain IDA [4–7]. The catalytic mechanism of DEA dehydrogenation has rarely been reported and is generally thought to be similar to the dehydrogenation mechanism of other fatty alcohols where esters are produced using Cu-based catalysts. The Cu-based catalysts catalyze the dehydrogenation of diethanolamine to form an intermediate aldehyde, followed by two molecules of aldehyde combining to form a carboxylic acid and an alcohol [8].

Cu-based catalysts are widely used in the dehydrogenation of alcohols to produce esters or aldehydes [9–14]. Excellent results for the selective conversion alcohols to esters have been achieved using Cu/ZrO₂ catalysts [15–20], and interfacial metal-support interactions between Cu and ZrO₂ enhances the dehydrogenation of ethanol to form ethyl acetate [18]. A CuO/ZrO₂ precursor was prepared by coprecipitation, followed by high-temperature reduction under an H₂ flow to obtain Cu/ZrO₂ catalysts [15, 19–21]. In addition to Cu⁰, a small amount of Cu⁺ in Cu/ZrO₂ catalysts plays an essential role in the selectivity of ethyl acetate in the dehydrogenation of ethanol [15]. The Cu content in CuO/ZrO₂ and CuO/SiO₂ during programmed temperature reduction were studied by X-ray absorption near edge structure (XANES), which showed that the copper in CuO underwent reduction via Cu²⁺ → Cu⁺ → Cu⁰ under an H₂ flow. When the Cu content in the catalysts is high, Cu⁰ is the

main species present, but when the Cu content is low, the amount of Cu in the ZrO₂ carrier is high, and the nearby oxygen vacancy makes it difficult to reduce Cu⁺ to Cu⁰ [22, 23]. The type of carrier also has a certain effect on the Cu⁰/Cu⁺ pair. As the amount of zinc oxide content increases in Cu/SiO₂ catalysts, the Cu⁺ content also increases [24]. Cu₂O provides active acidic sites (Lewis acid sites) on the surface of the catalysts which help promote the chemical adsorption capacity of intermediate aldehydes, thereby increasing the reaction rate and conversion of organic acids [15, 25]. Cu₂O/MgO has a better catalytic activity than Cu/MgO for the catalytic reaction of cyclohexanol for cyclohexanone production [26], suggesting that Cu⁺ and Cu⁰ have differences in their catalytic activities.

In the present paper, Cu/ZrO₂ catalysts were prepared by reducing CuO/ZrO₂ precursors with hydrazine hydrate. The best results obtained with this catalyst were a 98% yield of disodium iminodiacetate in a 2.3 h reaction time. Therefore, hydrazine hydrate is an excellent candidate to produce Cu/ZrO₂ catalysts. The effect of the Cu⁰/Cu⁺ pair on the catalytic reaction was studied by controlling the reduction degree of CuO/ZrO₂ precursors. It was found that increasing the Cu⁰ content favored the dehydrogenation of DEA to form intermediate aldehydes, and Cu⁺ promoted the reaction of an aldehyde intermediate to form iminodiacetate. The formation mechanism of sodium glycinate is related to the tautomerism of the intermediate products and the hydrolysis of a Schiff base.

2 Experimental

2.1 Catalyst Preparation

CuO/ZrO₂ precursor was synthesized by a co-precipitation method. Briefly, ZrOCl₂·8H₂O and Cu(NO₃)₂·3H₂O were dissolved in deionized water to obtain Cu/Zr in a molar ratio of 2:1. Then, 1.0 mol/L NaOH solution was added dropwise under continuous stirring to adjust the pH to 12. The resulting precipitate was aged at room temperature for 4 h. Next, the precipitate was filtered and washed by deionized water several times in a Buchner funnel until the pH value of the supernatant was neutral. The composite precursor was dehydrated and dried at 90 °C for 12 h. The resulting powder was calcined in a muffle furnace from room temperature to 550 °C at a ramp rate of 2 °C/min and a dwell time of 4 h to obtain the CuO/ZrO₂ precursor.

CuO/ZrO₂ precursor powder (10 g) was added to 100 ml of a 2 M NaOH solution in a round-bottom flask, and then heated to 50 °C under mechanical stirring. Subsequently, 0.75–15 mL hydrazine hydrate was added slowly into

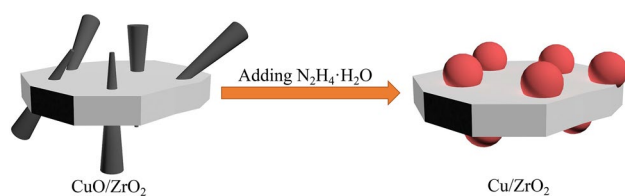


Fig. 1 Catalyst precursor reduction image

the above mixture, which continued to react at 50 °C for 10–60 min. Finally, the resulting composite was obtained after being filtered, washed with deionized water and ethanol several times, and dried in a vacuum oven at 40 °C for 12 h. Figure 1 is the reduction diagram of catalyst precursor.

2.2 Catalytic Test

The dehydrogenation reaction of DEA was carried out in a stainless steel autoclave. The initial reagents, including 31.5 g DEA, 6 g Cu/ZrO₂ catalyst, 25.2 g NaOH (dissolved in 64.8 g deionized water), were added to the autoclave. After the autoclave was purged with N₂, it was pressurized to 0.5 MPa, heated to 160 °C at a rate of 4 °C/min at a speed of 400 rpm, and the volume of gas generated during the reaction was measured by a rotor flow meter. When the pressure reached 1.5 MPa, the exhaust valve was opened to release the gas until the pressure decreased to 1 MPa, and the temperature and volume of each exhaust was recorded. The pressure increased by no more than 0.5 MPa within 20 min, which indicated that the reaction was complete.

3 Results and Discussion

3.1 Characterization and Analysis of Cu/ZrO₂ Catalysts

Figure 2 shows the X-ray diffraction (XRD) patterns of pure ZrO₂ supports, the CuO/ZrO₂ precursor, and the Cu/ZrO₂ catalysts reduced using different amounts of hydrazine hydrate. In this figure, X in Cu/ZrO₂-X represents the addition of X ml of 80 wt% hydrazine hydrate aqueous solution. The preparation method is described in Sect. 2.1, using a reduction time of 60 min. ZrO₂ was prepared through the same procedure for the CuO/ZrO₂ precursor, but without the addition of copper salt solution.

As shown in Fig. 2, pure ZrO₂ exhibits diffraction peaks which correspond to tetragonal (t-) and monoclinic (m-) ZrO₂ crystal phases. However, the CuO/ZrO₂ precursor only contains t-ZrO₂, indicating that the zirconium salt and copper salt solutions in the above co-precipitation reaction

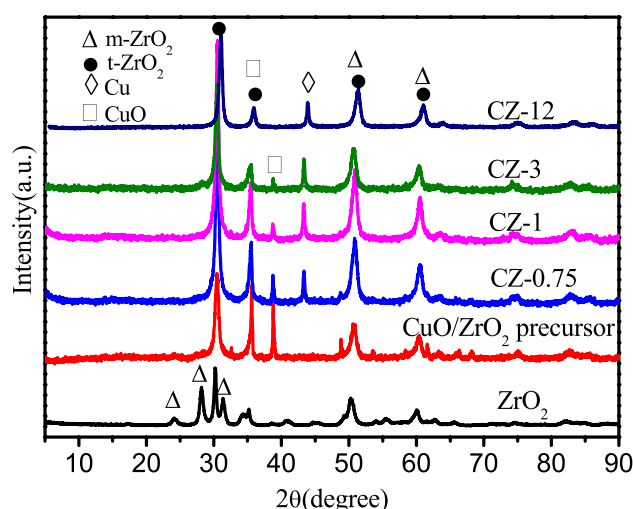


Fig. 2 XRD patterns of reduced Cu/ZrO₂ catalysts (X in CZ-X represents the volume of hydrazine hydrate used in the reduction of the precursors)

participate in transforming ZrO₂ from a monoclinic to a tetragonal phase. The CuO/ZrO₂ precursor exhibits CuO diffraction peaks without Cu⁰ characteristic peaks. As the amount of hydrazine hydrate increased, the main CuO diffraction peaks ($2\theta = 35.5^\circ, 38.7^\circ$) in Cu/ZrO₂ weakened, and characteristic Cu⁰ peaks appeared at $2\theta = 43.3^\circ$. When the amount of hydrazine hydrate increased to 12 mL, the main CuO diffraction peak ($2\theta = 35.5^\circ$) disappeared, indicating that a higher amount of hydrazine hydrate led to a higher reduction degree of Cu/ZrO₂. The Cu⁺ diffraction peaks were not detected in the XRD spectra, possibly because the Cu⁺ content was lower than the XRD detection limit [27].

The catalyst morphology was characterized by scanning electron microscopy (SEM) and transmission electron microscopy (TEM). Figure 3a, b shows the SEM images of the unreduced CuO/ZrO₂ catalyst precursor, in which needle-like CuO is inserted into an irregular bulk ZrO₂ support. Figure 3c, d are the SEM images of the Cu/ZrO₂ catalyst after hydrazine hydrate reduction, and Fig. 3e, f are the corresponding TEM images. Rod-shaped CuO was reduced to spherical Cu particles using hydrazine hydrate. Cu nanoparticles with a particle size of about 15 nm were uniformly distributed on the surface of the irregular bulk ZrO₂ support, indicating that hydrazine hydrate reduced CuO to Cu to successfully prepare the Cu/ZrO₂ catalyst.

To study the surface composition of the catalysts, Cu/ZrO₂ catalyst samples were characterized by Fourier-transform infrared spectroscopy (FTIR). Figure 4 is the FTIR image of the sample. The band at 3419 cm⁻¹ was attributed to the -OH stretching vibration of adsorbed water molecules, the band at 1624 cm⁻¹ was attributed to the -OH bending vibration of free water molecules, whereas the small bands

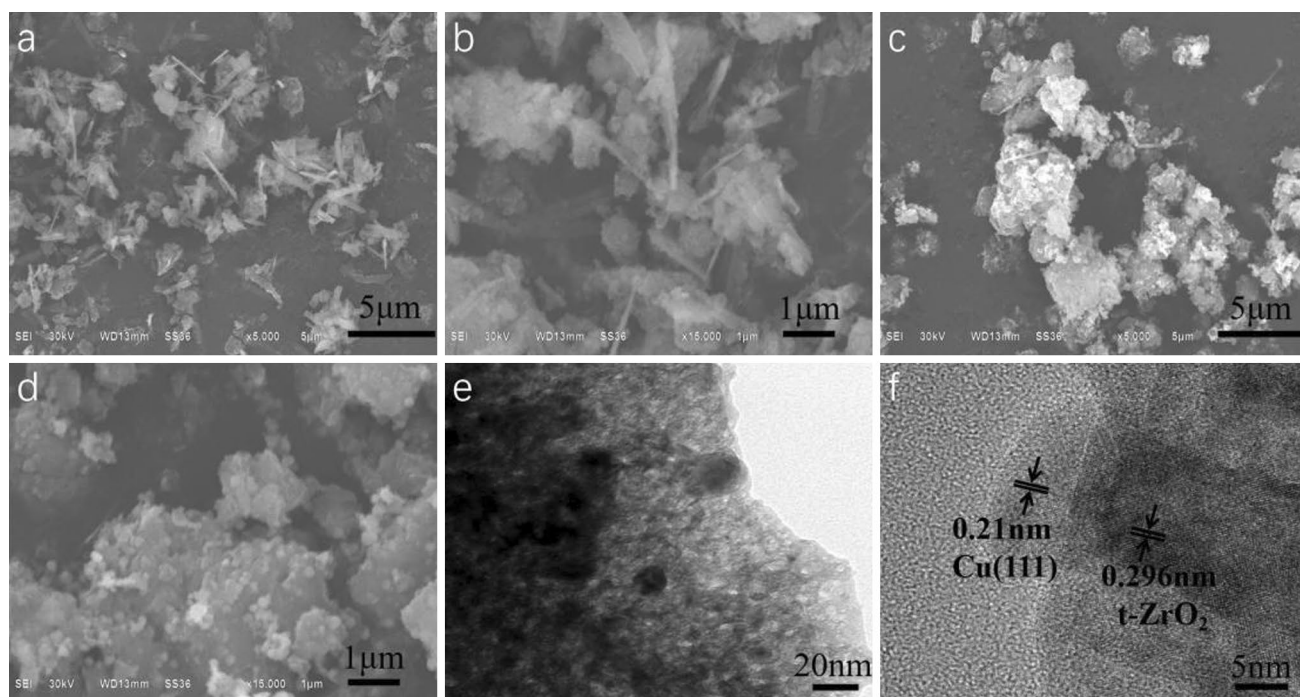


Fig. 3 SEM images of unreduced CuO/ZrO₂ (a, b), Cu-ZrO₂ (c, d); and TEM images of Cu-ZrO₂ (e, f)

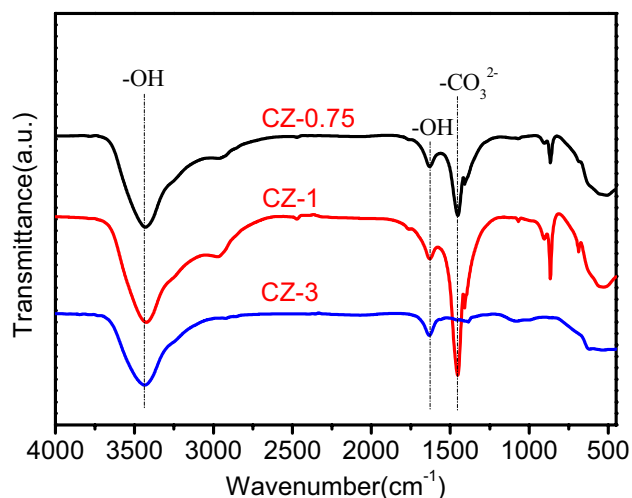


Fig. 4 FTIR spectra of the Cu/ZrO₂ catalysts

at 1450 and 853 cm⁻¹ were due to the various vibrational modes of carbonate. In addition, the stretching vibration of the CO₃²⁻ group in the CZ-1 sample was the most intense, indicating a large amount of CO₂ had adsorbed on the Lewis basic sites of CZ-1 to form a bicarbonate.

The surface composition and oxidation state of the catalyst components were investigated by XPS. The XPS spectra of Cu 2p and Auger electron spectra of Cu/ZrO₂ samples reduced by 0.75 mL (CZ-0.75), 1 mL (CZ-1), and 3 mL

(CZ-3) hydrazine hydrate are shown in Fig. 5a and b, respectively. The preparation method was as described in Sect. 2.1, and the reduction time was 60 min.

All Cu 2p spectra contain a large satellite peak near 940–944 eV, which suggests there is a large amount of Cu²⁺ on the surface of the catalysts [29–31]. Depending on the effective symmetry, copper ions may transition to 3d. Therefore, a complex satellite structure composed of at least two peaks was clearly visible in the Cu 2p spectrum may be due to the distortion of the octahedral structure of the copper compound [28]. Peaks at 932.2 eV were assigned to Cu⁰ and Cu⁺, and cannot be effectively distinguished from the XPS Cu 2p peak since they are so close to each other. Additionally, characteristic Cu²⁺ peaks appear at 934.4 eV. As the amount of hydrazine hydrate was increased, the peak intensity of Cu⁰/Cu⁺ increased, indicating that the reduction degree of the catalysts also increased, which is consistent with the XRD spectra.

Figure 5b shows the Auger electron spectra of the Cu/ZrO₂ catalysts. The three peaks with Auger electron kinetic energies of 916.3 eV, 917.4 eV, and 918.4 eV correspond to Cu⁺, Cu²⁺, and Cu⁰, respectively [29]. Table 1 shows the surface copper components based on Cu LMM deconvolution and surface atomic ratios of Zr and O versus Cu based on XPS analysis. It can be concluded that increasing the amount of hydrazine hydrate lowered the amount of Cu²⁺ on the catalyst surface, while the proportion of Cu⁰ and Cu⁺ increased. Combined with the catalyst activity test, when

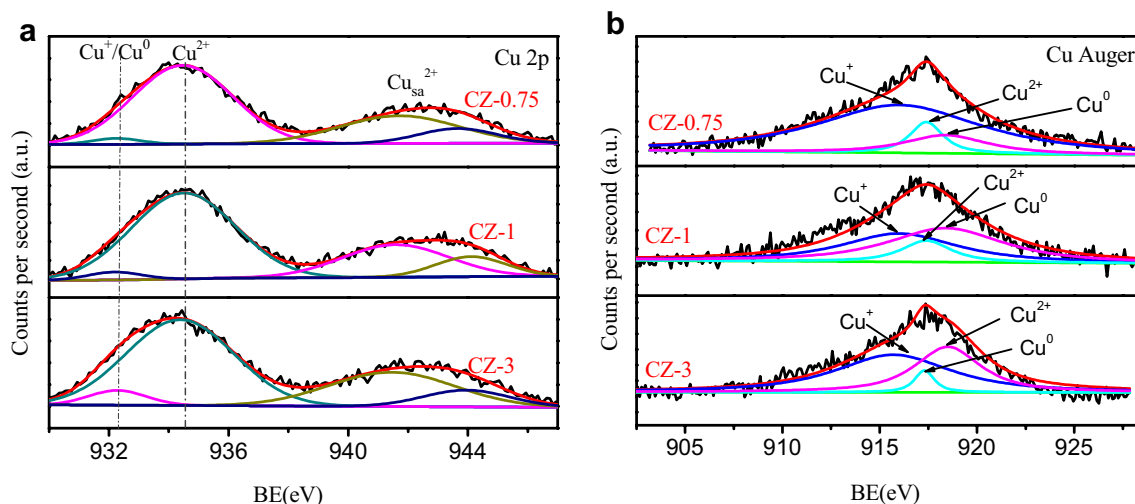


Fig. 5 XPS spectra of Cu 2p (a), and Auger electron spectra (b) of reduced Cu/ZrO₂ samples

Table 1 Surface copper components based on Cu LMM deconvolution and surface atomic ratios of Zr and O versus Cu based on XPS analysis

Samples	Kinetic energies (eV)			Peak area ratio ^a Cu ⁰ :Cu ⁺ :Cu ²⁺	Atomic content ^b /%		
	Cu ⁰	Cu ⁺	Cu ²⁺		Cu	Zr	O
CZ-0.75	918.4	916.0	917.4	1:5.27:0.68	24.1	15.2	60.7
CZ-1	918.4	916.0	917.4	1:0.89:0.27	28.6	11.8	59.6
CZ-3	918.5	915.8	917.3	1:1.44:0.15	26.4	12.3	61.3
t-20	918.4	916.0	917.4	1:2.17:0.49	28.5	12.1	59.4
t-30	918.4	916.0	917.4	1:0.97:0.15	24.1	13.9	62.0
t-40	918.4	916.0	917.4	1:7.49:1.43	23.3	14.8	61.9

^aPeak area ratios between Cu²⁺, Cu⁺, and Cu⁰ were calculated by the deconvolution of Cu LMM XAES

^bAtomic ratios of Cl to Cu were obtained by XPS analysis

1 ml of hydrazine hydrate was used, the catalyst showed the best activity when the ratio of Cu⁰/Cu⁺ was 1:0.89.

Figure 6 shows the preparation of Cu/ZrO₂ catalysts with 1 mL hydrazine hydrate with reduction times of 20 min (t-20), 30 min (t-30), and 40 min (t-40). As the reduction time increased, the peaks representing Cu⁰ and Cu⁺ increased first and then weakened. According to the Auger electron spectra, the proportion of Cu⁰ increased first and then decreased, while the proportion of Cu²⁺ decreased first and then increased. It is presumed that Cu⁺ and Cu⁰ were produced by the reduction of Cu²⁺ with hydrazine hydrate, and the reduction degree was the highest at a reduction time of 30 min. As the reaction continued, the amount of hydrazine hydrate in the solution decreased, and Cu⁺ and Cu⁰ was oxidized to form Cu²⁺ at a moderate temperature of approximately 50 °C. According to the catalyst activity test, when

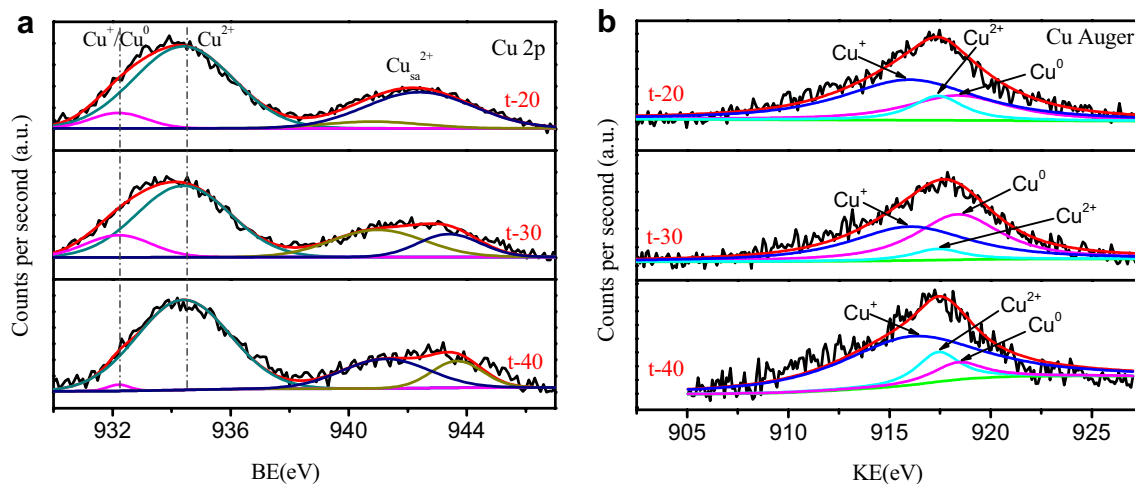


Fig. 6 XPS spectra of Cu 2p (a), and Auger electron spectra (b) of reduced Cu/ZrO₂ samples

the hydrazine hydrate reduction time was 30 min, the catalytic activity was best when the ratio of Cu^0/Cu^+ was 1:0.97.

In order to analyze the Lewis basic sites of the catalyst surface, the characterization of CO_2 -TPD was performed on samples reduced with different amounts of hydrazine hydrate (Fig. 7). All three catalyst samples exhibited a CO_2 desorption peak at 99 °C, which corresponded to the weakly basic sites [32]. In addition to the weakly basic sites, the desorption peak at 260 °C can be assigned to medium-strength Lewis basic sites (MSLB) [33, 34]. In the CZ-1 sample, the MSLB dominated the sample, which indicates that the use of different amounts of hydrazine hydrate can change the amount of Lewis basic sites on the catalyst. Combined with the catalyst performance test, it can be seen an increase in the MSLB improved the efficiency of the dehydrogenation of diethanolamine.

3.2 Catalytic Activity

Figure 8 shows that the higher the yield of IDA, the shorter the required reaction time. As the reduction degree of the catalysts increased, the IDA yield first increased and then decreased, reaching a maximum yield of 92.7% when using 1 mL of reductant.

The relationship between the IDA yield and reaction time and the reduction time of the catalysts is shown in Fig. 9. The preparation method is as described in Sect. 2.1, and 1 mL of hydrazine hydrate was used.

The IDA yield first increased and then decreased with the catalyst reduction time, and the maximum yield of IDA (98.1%) was obtained at t-30. The XPS analysis of the catalysts showed that the ratio of Cu^+/Cu^0 had an important effect on the reaction yield. Figure 6c shows that when different reduction times are used, the ratio of Cu^+/Cu^0 is also

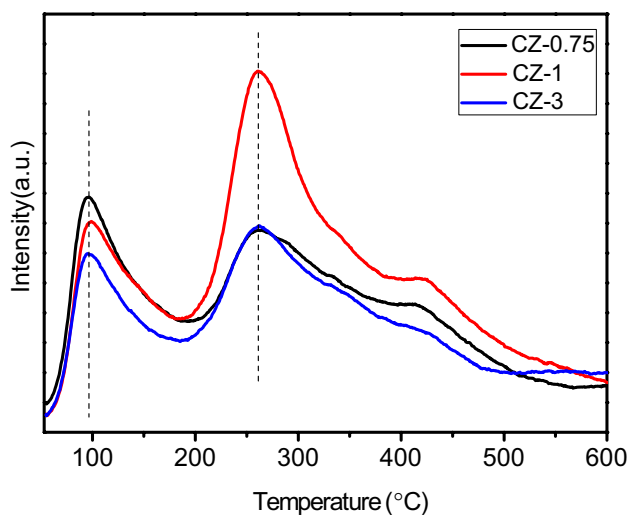


Fig. 7 CO_2 -TPD profiles for the samples

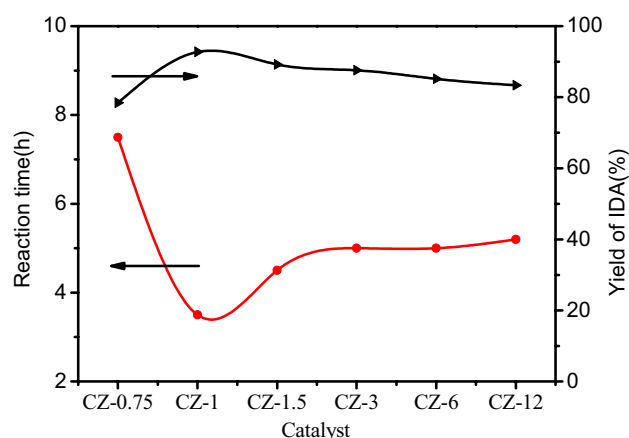


Fig. 8 The relationship between the reducing agent used to prepare the catalysts and the IDA yield and the reaction time (X in CZ-X represents the volume of hydrazine hydrate used in catalyst reduction)

different, as is the catalytic effect. Combined with Fig. 9, it can be seen that the sample reduced by hydrazine hydrate for 30 min had the highest Cu^+/Cu^0 , the shortest reaction time, and the highest IDA yield.

The ester preparation process by the dehydrogenation of fatty alcohol occurred in two steps: alcohol dehydrogenation to produce an aldehyde, and ester production from the reaction between an aldehyde and an alcohol [16, 17]. It can be seen from Figs. 5 and 6 that as the amount of hydrazine hydrate increased, the Cu^0 and Cu^+ content gradually increased.

Figure 10 shows the relationship between the amount of hydrazine hydrate used to prepare the catalysts and the reaction temperature at the first exhaust. The lowest temperature of the first exhaust was recorded at CZ-1, and then the initial exhaust temperature rose, and then decreased as

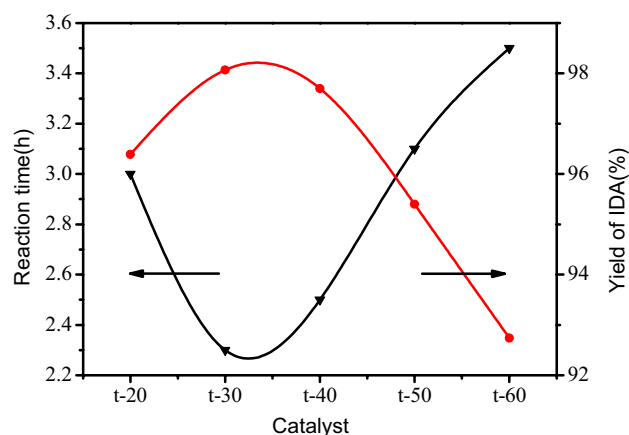


Fig. 9 The relationship between the reduction time of the prepared catalyst and the reaction time and yield of IDA (X in t-X represents the reduction time of the prepared catalysts)

more hydrazine hydrate was added. When more than 3 mL of hydrazine hydrate was added, the initial temperature of the exhaust gas rapidly decreased, but the overall reaction time was longer. When 1 mL of hydrazine hydrate was used, the initial exhaust temperature was the lowest, and the reaction rate was the fastest, as shown in Fig. 6. The Cu⁰ and Cu⁺ content in the catalysts was not the highest compared with other catalysts, indicating that the Cu⁰/Cu⁺ pair reached the optimum ratio when 1 mL hydrazine hydrate was used.

The results of the above reactions show that Cu⁰ catalyzes the first step in the DEA dehydrogenation reaction to form an intermediate aldehyde, and Cu⁺ has excellent catalytic activity for the reaction of the intermediate aldehyde. As the Cu⁰ content increased, the temperature of the first exhaust gas decreased, the speed of the early exhaust accelerated, but the rate of the subsequent reaction quickly decreased. It should be noted that Cu⁰ does not catalyze the entire reaction to prepare disodium iminodiacetate from DEA as described in the literature [5]. Increasing the Cu⁰ content accelerated the initial reaction rate and decreased the temperature of the primary exhaust. However, as the reaction proceeded, the reaction rate decreased since the intermediate aldehyde could not be transformed via Cu⁰ catalysis. When 1 mL of hydrazine hydrate was used, the Cu⁰/Cu⁺ pair in the catalysts reached the optimum ratio, and Cu⁺ catalyzed the intermediate aldehyde generated in the first step to produce disodium iminodiacetate. There was no accumulation of intermediate aldehyde, and the first step of the reaction was rapid, which decreased the overall reaction time.

During the initial stage of diethanolamine dehydrogenation using CZ-1 catalyst, the temperature inside the kettle rose rapidly and reached a peak at 230 °C and then rapidly dropped to 120 °C. In contrast, the temperature was constant at 165 °C when using CZ-6 and CZ-12. The alcohol

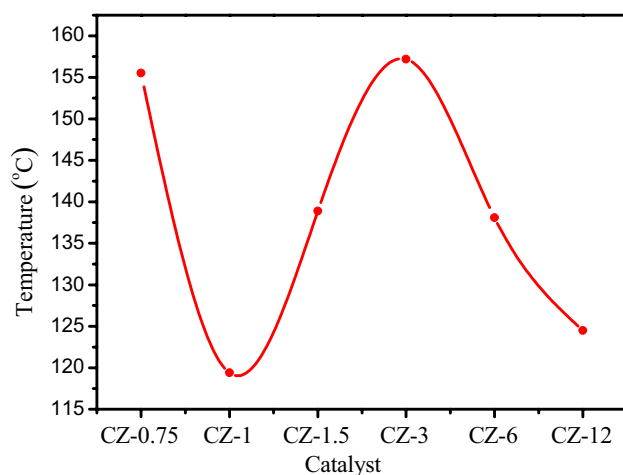


Fig. 10 Relationship between the amount of reducing agent used to prepare the catalysts and temperature at the first exhaust (X in CZ-X represents the volume of hydrazine hydrate used in catalyst reduction)

dehydrogenation reaction is endothermic, while the reaction between the ester and NaOH is exothermic. When the rate of the entire reaction is very fast, the heat provided by the autoclave is not sufficient to drive the alcohol dehydrogenation reaction, and the temperature rapidly decreases. The ester formation rate simultaneously increased, and NaOH reacted with it immediately to release a significant amount of heat which increased the temperature from its set value of 160 °C to almost 190 °C. These processes may be the cause of the sudden temperature increase.

3.3 Formation Mechanism of Disodium Iminodiacetate and Sodium Glycine

3.3.1 Formation Mechanism of Disodium Iminodiacetate

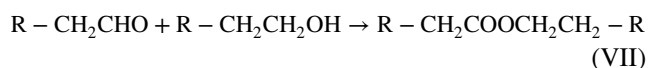
In the dehydrogenation of homogeneous alcohols, organic bases or other basic compounds are often used as additives to accelerate the deprotonation of the hydroxyl group to achieve high yields of the target product. Similarly, in heterogeneous catalytic reactions, basic compounds improve the catalytic activity of alcohol transfer dehydrogenation. In the Cu–ZrO₂ catalyst, the ZrO₂ carrier has a Lewis basic site, and the Cu–ZrO₂ catalyst reduced by 1 ml of hydrazine hydrate had the most Lewis basic sites and exhibited better diethanolamine dehydrogenation performance. Therefore, the transfer efficiency of diethanolamine in Cu–ZrO₂ catalyst is related to its surface Lewis basic sites.

The mechanism for the preparation of disodium iminodiacetate from DEA has rarely been reported. Similar to the reaction of monoethanolamine during the preparation of glycine [35], it is generally believed that DEA is dehydrogenated to produce aldehyde intermediates using Cu-based catalysts. Then, two aldehyde molecules form sodium iminodiacetate in an alkaline medium [8]. However, the active center of Cu/ZrO₂ catalysts and the ester formation process from aldehydes are unclear.

The Cu/ZrO₂ catalyzed dehydrogenation of DEA occurs in two steps, similar to the mechanism of fatty alcohol dehydrogenation over Cu-based catalysts. The hydroxyl functional groups on the DEA are first removed via nucleophilic attack of the Lewis basic sites at the ZrO₂ interface to form an alkoxide intermediate, and an alkaline solution can accelerate the rate of deprotonation [36]. Subsequently, the adjacent Cu⁰ catalyzes the formation of the intermediate aldehyde by α -H cleavage [20, 37, 38].

The reaction process to prepare an ester from aldehydes has two possible reaction routes: (VI) the Cannizzaro reaction between two aldehydes, and (VII) the nucleophilic addition of aldehydes and alcohols:





In the first route, the Cannizzaro reaction cannot produce the corresponding ester [39]. When the aldehyde in the reactants contains an α -H, it is extracted by the base, and aldol condensation occurs [16], which prevents the synthesis of disodium iminodiacetate by DEA dehydrogenation from following this route. In the second route, the α -H on the aldehyde of the intermediate is removed by the alkali, causing the electrophilic α -C to react with an alkoxide to form an ester [40]. In an alkaline environment, the ester decomposes to form disodium iminodiacetate and DEA. Compared with Cu^0 , Cu^+ has better catalytic activity for the nucleophilic

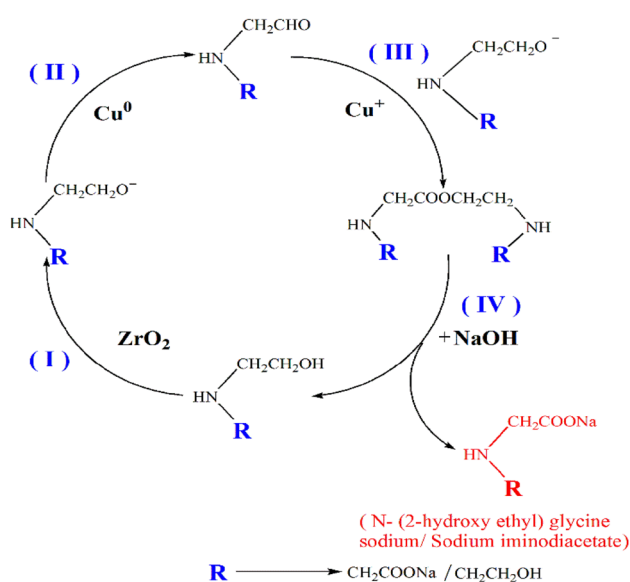


Fig. 11 Formation mechanism of disodium iminodiacetate

addition of alcohols and aldehydes [15]. The formation mechanism of disodium iminodiacetate is shown in Fig. 11.

3.3.2 Formation Mechanism of Sodium Glycine

Sodium glycine is the main by-product in the preparation of disodium iminodiacetate by DEA dehydrogenation, and its formation mechanism has not been reported. Gas chromatography analysis revealed that the gas produced during the reaction contained acetaldehyde. Combined with high performance liquid chromatography to analyze crude products, the formation mechanism of sodium glycine is divided into the acetaldehyde route and glycolaldehyde route.

3.3.2.1 Acetaldehyde Route Acetaldehyde was identified by gas chromatography during the reaction, and the mechanism of the main by-product sodium glycine was speculated. The Cu/ZrO_2 used to catalyze the dehydrogenation of DEA and the ZrO_2 support contain weakly acidic and basic sites, respectively [21, 41]. Cu/ZrO_2 catalyzes the dehydrogenation of alcohol (I) to form olefins, followed by the formation of a Schiff base via enamine-imide tautomerism (II). As the reaction proceeds, the basicity of the reaction system gradually weakens. At high temperatures, the Schiff base produces acetaldehyde and sodium glycinate by hydrolysis (III). The formation mechanism is shown in Fig. 12.

3.3.2.2 Glycolaldehyde Route The dehydrogenation (IV) of DEA using Cu/ZrO_2 catalysts produces intermediate aldehydes and forms a Schiff base by keto-enol tautomerism (V) and an enamine-imine tautomer (VI). The Schiff base produces the main glycine and glycolaldehyde byproducts through a hydrolysis reaction (VII). Due to the catalytic activity of Cu/ZrO_2 towards hydroxyl and aldehyde groups,

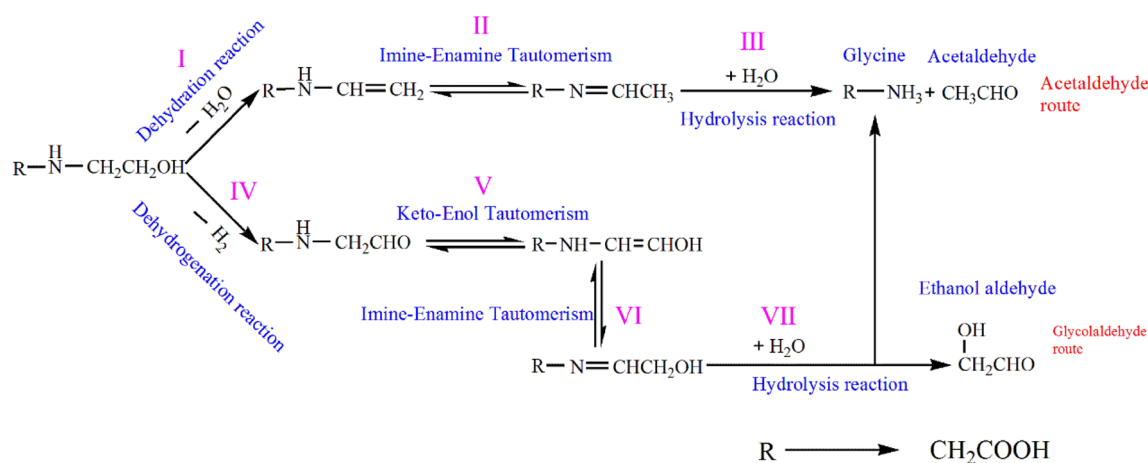


Fig. 12 The formation mechanism of sodium glycine

glycolaldehyde is oxidized to form the glycolic acid and oxalic acid intermediate byproducts [6, 42]. The formation mechanism is shown in Fig. 12.

4 Conclusion

In this paper, Cu/ZrO₂ catalysts were rapidly prepared by hydrazine hydrate reduction at a moderate temperature from CuO/ZrO₂ precursors. The catalysts could also be used in the oxidative dehydrogenation of diethanolamine to prepare disodium iminodiacetic acid. Adding more hydrazine hydrate in the preparation increased the Cu⁰ content in Cu/ZrO₂, but the yield of sodium iminodiacetate synthesized via diethanolamine dehydrogenation increased with the Cu⁰ content in the catalysts. When the Cu⁰/Cu⁺ ratio is approximately 1:0.9, the highest catalyst activity was observed. The abovementioned results indicate that Cu⁰ was the catalytic active center when diethanolamine dehydrogenation was used to obtain disodium iminodiacetic acid, which conflicts with previous literature. XPS and XRD were used to analyze the structure and reaction results of the Cu/ZrO₂ catalysts, and showed that Cu⁰ played a key role in the first step of the dehydrogenation of diethanolamine to form intermediate aldehydes. Meanwhile, Cu⁺ was also essential for transforming intermediate aldehydes into disodium iminodiacetic acid. The formation mechanism of glycine, the main by-product of diethanolamine dehydrogenation, was also proposed for the first time. By analyzing the presence of acetaldehyde in the gases produced by the reaction, it was surmised that intermediate aldehydes or alkenes underwent keto-enol tautomerism and imine-enamine tautomerism, to generate a Schiff base, followed by hydrolysis to produce the main by-products sodium glycinate, sodium glycolate, and sodium silicate. This mechanism is proposed to improve the yield of the main product, iminodiacetic acid, and guide the optimization of the process conditions.

Acknowledgements Support from the National Natural Science Foundation of China (Grant No. NSFC 21576229) is gratefully acknowledged.

Compliance with Ethical Standards

Conflict of interest The authors declare that they have no conflicts of interest.

References

- Alibhai MF, Stallings WC (2001) Proc Natl Acad Sci USA 98:2944–2946
- Chen D, Li J, Li GR, Chen BH, Yin FX (2013) Chem Ind Eng Prog 32:1635–1640
- Andreev DV, Sergeev EE, Gribovskii AG, Makarshin LL, Prikhod'ko SA, Adonin NY, Pai ZP, Parmon VN (2017) Chem Eng J 330:899–905
- Zheng XJ, Yang GW, Xu XX, Yang G (2001) Fine Chem 18:608–610
- Wang Y, Zhao Y, Zhao Z, Lan X, Xu J, Xu W, Duan Z (2019) Acta Chim Sin 71:661–668
- Hickman DA, Mosner K, Ringer JW (2015) Chem Eng J 278:447–453
- Andreev DV, Gribovskii AG, Makarshin LL, Adonin NY, Prikhod'ko SA, Pai ZP, Parmon VN (2013) Catal Ind 5:1–8
- Yang AS, Pan YF, Sun Q, Cheng R, Zheng YP, Xu GM (2010) J Chem Eng Chin Univ 4:590–595
- Lu Z, Gao D, Yin H, Wang A, Liu S (2015) J Ind Eng Chem 31:301–308
- Nagaiah P, Venkat Rao M, Thirupathaiiah K, Venkateshwarlu V, David Raju B, Rama Rao KS (2018) Res Chem Intermed 44:5817–5831
- Yin H, Yin H, Wang A, Shen L, Liu Y, Zheng Y (2017) J Nanosci Nanotechnol 17:1255–1266
- Sun D, Mitsu T, Yamada Y, Sato S (2019) Appl Catal A. <https://doi.org/10.1016/j.apcata.2019.06.007>
- Ohira M, Liu H, He D, Hirata Y, Sano M, Suzuki T, Miyake T (2018) J Jpn Petrol Inst 61:205–212
- Gao D, Yin H, Wang A, Shen L, Liu S (2015) J Ind Eng Chem 26:322–332
- Wang LX, Zhu WC, Zheng DF, Yu X, Cui J, Jia MJ, Zhang WX, Wang ZL (2010) React Kinet Mech Catal 101:365–375
- Inui K, Kurabayashi T, Sato S (2002) J Catal 212:207–215
- Inui K, Kurabayashi T, Sato S (2002) Appl Catal A 237:53–61
- Ro I, Liu YF, Ball MR, Jackson DHK, Chada JP, Sener C, Kuech TF, Madon RJ, Huber GW, Dumesic JA (2016) ACS Catalysis 6:7040–7050
- Zonetti PC, Celnik J, Letichevsky S, Gaspar AB, Appel LG (2011) J Mol Catal A 334:29–34
- Sato AG, Volanti DP, Freitas IC, Longo EI, Bueno JC (2012) Catal Commun 26:122–126
- Bai GY, Wang YL, Li F, Zhao Z, Chen GF, Li N, Han X (2012) Catal Lett 143:101–107
- Freitas IC, Damyanova S, Oliveira DC, Marques CMP, Bueno JMC (2014) J Mol Catal A 381:26–37
- Chen CQ, Ruan CX, Zhan YY, Lin XY, Zheng Q, Wei KM (2014) Int J Hydrogen Energy 39:317–324
- Ji DH, Zhu WC, Wang ZL, Wang GJ (2007) Catal Commun 8:1891–1895
- Hu Q, Fan GL, Yan L, Cao XZ, Zhang P, Wang BY, Li F (2016) Green Chem 18:2317–2322
- Shi QJ, Liu N, Liang Y (2007) Chin J Catal 28:57–61
- Komandur VR, Guggilla VS, Chakravarthula SS, Vattikonda VR (2007) J Phys Chem B 11:543–550
- Kim S (1974) J Electron Spectrosc Relat Phenom 3:217–226
- Severino F, Brito JL, Laine J, Fierro JL, Lopez Agudo A (1998) J Catal 177:82–95
- Acharyya SS, Ghosh S, Bal R (2014) ACS Sustain Chem Eng 2:584–589
- Maiti S, Llorca J, Dominguez M, Colussi S, Trovarelli A, Priolkar KR, Aquilanti G, Gayen A (2016) J Power Sources 304:319–331
- Unnikrishnan P, Srinivas D (2012) Ind Eng Chem Res 51:6356–6363
- Hu Q, Yang L, Fan GL, Li F (2016) Chem Nano Mat 2:888–896
- Wang J, Lei Z, Qin H, Zhang L, Li F (2011) Ind Eng Chem Res 50:7120–7128
- Yang YC, Duan ZK, Liu WY, Li GL, Xiong Y (2001) Chem React Eng Technol 17:210–215

36. Balaraman E, Khaskin E, Leitus G, Milstein D (2013) *Nat Chem* 5:122–125
37. Zhang M, Zhao YJ, Liu Q, Yang L, Fan GL, Li F (2016) *Dalton Trans* 45:1093–1102
38. Wang ZY, Liu XY, Rooney DW, Hu P (2015) *Surf Sci* 640:181–189
39. Takeshita K, Nakamura S, Kawamoto K (1978) *Bull Chem Soc Jpn* 51:2622–2627
40. Neurock M, Tao ZY, Chemburkar A, Hibbitts DD, Iglesia E (2017) *Faraday Discuss* 197:59–86
41. Manríquez ME, López T, Gómez R, Navarrete J (2004) *J Mol Catal A* 220:229–237
42. Jiang ZW, Zhang ZR, Song JL, Meng QL, Zhou HC, He ZH, Han BX (2016) *ACS Sustain Chem Eng* 4:305–311

Publisher's Note Springer Nature remains neutral with regard to jurisdictional claims in published maps and institutional affiliations.

Affiliations

Yongsheng Wang^{1,2} · Hongwen Zhu¹ · Zhengkang Duan^{1,2} · Zhenzhen Zhao^{1,2} · Yunlu Zhao^{1,2} · Xiaolin Lan¹ · Li Chen¹ · Dongjie Guo¹

Yongsheng Wang
871585227@qq.com

Hongwen Zhu
zhw3255805@qq.com

Zhenzhen Zhao
1098808414@qq.com

Yunlu Zhao
1820955484@qq.com

Xiaolin Lan
1107300386@qq.com

Li Chen
1062785680@qq.com

Dongjie Guo
1457555605@qq.com

¹ College of Chemical Engineering, Xiangtan University, Xiangtan 411100, China

² Hunan Collaborative Innovation Center of New Chemical Technologies for Environmental Benignity and Efficient Resource Utilization, Xiangtan 411105, Hunan, China